

## NUMERICAL SIMULATION OF FLOWS IN THE PRESENCE OF MOVING BOUNDARIES USING THE IMMERSED BOUNDARY METHOD

### Juliano Marcelo de Arruda

Faculdade de Engenharia Mecânica  
Universidade Federal de Uberlândia  
Campus Santa Mônica, Uberlândia, Brasil  
[jmarruda@mecanica.ufu.br](mailto:jmarruda@mecanica.ufu.br)

### Ana Lúcia Fernandes de Lima e Silva

Faculdade de Engenharia Mecânica  
Universidade Federal de Uberlândia  
Campus Santa Mônica, Uberlândia, Brasil  
[alfernandes@mecanica.ufu.br](mailto:alfernandes@mecanica.ufu.br)

### Aristeu da Silveira Neto

Faculdade de Engenharia Mecânica  
Universidade Federal de Uberlândia  
Campus Santa Mônica, Uberlândia, Brasil  
[aristeus@mecanica.ufu.br](mailto:aristeus@mecanica.ufu.br)

### Alexandre Megiorin Roma

Instituto de Matemática e Estatística  
Universidade de São Paulo  
Cidade Universitária, São Paulo, Brasil  
[roma@ime.usp.br](mailto:roma@ime.usp.br)

**Abstract:** *The Immersed Boundary Method is used to model the walls bounding flows in channel and driven cavities. In this method a force source term is added to the Navier-Stokes equations, in order to model and guarantee the non-slipping boundary conditions at the channel and cavities walls. The Physical Virtual Model (PVM), which is a methodology proposed by the LTCM – FEMEC research group, is used to model the force field. This methodology employs the Navier-Stokes equations to compute the interfacial force presented in the flow. Preliminary results for the Couette-Poiseuille flow and driven cavity are presented.*

**Key-words:** *Immersed boundary, moving boundary, force source term, channel, driven cavity.*

## 1. INTRODUCTION

Engineering problems involving fluids flows in complex geometries are very usual, and the major difficulty arise in how to represent the body geometrically complex, its moving walls and its interaction with the fluid.

The most usual approach is using Neumann and Dirichlet boundaries conditions to represent the body geometry. Therefore if the geometry is complex it is a hard and, probably, a very difficult work. This difficulty grows up if the body has a moving and deformable geometry.

Some authors have proposed different methods to treat this kind of problem. Harlow & Welch (1965) proposed the Marker and Cell (MAC). In this method the fluid region in on side of the boundary is identified by markers, while the other side of the boundary, which can be fluid or solid, is identified by another marker. Peskin (1977) proposed his Immersed Boundary Method, in which the interface between fluid and body is represented by a lagrangean mesh, that interacts with the flows domain, represented by an eulerian mesh. A force term added to the Navier-Stokes equation is in charge to promote the interaction between these meshes. Different ideas have been proposed to calculate this force term.

Peskin's original idea was based in Hooke's Law of Elasticity. In this model the lagrangean nodes,  $\mathbf{X}_k$ , are connected by springs of constant  $k \gg 1$ , to a equilibrium point  $\mathbf{X}^e$ . Goldstein *et al.* (1993) proposed the Virtual Boundary Formulation. In this method the force term is obtained with the sum of inercial forces over a massless body. Both methods deals with *ad-hoc* constants, which must to be fitted for each case.

Fadlun *et al.* (2000) used the Navier-Stokes equation to calculate the force term in the first external grid point, using its velocity. Therefore it is necessary an algorithm to identify the grid points that must be calculate.

Lima e Silva *et al.* (2002) proposed a method named Physical Virtual Model (PVM), in which the force term is calculated over a sequence of lagrangean points using the Navier-Stokes equation. Using the same methodology Arruda et al (2002) simulated two types of channel flows: Couette, for moderate Re values (100 - 1000) and Couette-Poiseuille, for low Re values (10 - 100).

In the present work we simulate, using the PVM, two types of flow. Preliminary results are present for Couette-Poiseuille flow and the driven cavity flow. For the Couette-Poiseuille flow the quantities, velocity, force and friction coefficient are presented for  $Re = 250$  ( $Re$  is defined upon the mean velocity and the channel highness). It also presented velocities profiles and frictions coefficients comparison for different  $Re$  numbers. For the driven cavity the streamlines, pressure and vorticity fields, and the velocity profiles for  $Re = 400$  and  $1000$ , are presented.

## 2. MATHEMATICAL FORMULATION

### 2.1. Governing equations

Incompressible, laminar, isothermal and newtonian fluid flows in a rectangular domain  $\Omega$  were considered. The governing equations are mass conservation and Navier-Stokes. They can be written as:

$$\bar{\nabla} \cdot \bar{V} = 0, \quad (1)$$

$$\rho \left[ \frac{\partial \bar{V}}{\partial t} + (\bar{V} \cdot \bar{\nabla}) \bar{V} \right] = -\bar{\nabla} p + \bar{\nabla} \cdot \left[ \nu (\bar{\nabla} \bar{V} + \bar{\nabla}^T \bar{V}) \right] + \bar{F} \quad (2)$$

where  $\nu$  is the kinematic viscosity, and  $\bar{F}$  is an force term, which will be explained at the next topic.

### 2.2. Physical virtual model

The force term  $\bar{F}$ , that differs from zero only over the boundary, represents the eulerian force field and it is given by:

$$\bar{F}(\bar{x}) = \int_{\Omega} \bar{f}(\bar{x}_k) \delta(\bar{x} - \bar{x}_k) d\bar{x}_k, \quad (3)$$

where  $\bar{x}_k$  are the lagrangean grid points,  $\bar{f}(\bar{x}_k)$  is the lagrangean force density e  $\delta(\bar{x} - \bar{x}_k)$  is a Dirac delta function. The lagrangean force is calculated by the Navier-Stokes equation, and it can be expressed by

$$\bar{f}(\bar{x}_k) = \bar{f}_a(\bar{x}_k) + \bar{f}_i(\bar{x}_k) + \bar{f}_v(\bar{x}_k) + \bar{f}_p(\bar{x}_k), \quad (4)$$

where,

$$\bar{f}_a(\bar{x}_k) = \rho \frac{\partial \bar{V}(\bar{x}_k)}{\partial t}, \quad (5)$$

$$\bar{f}_i(\bar{x}_k) = \rho (\bar{V} \cdot \bar{\nabla}) \cdot \bar{V}(\bar{x}_k), \quad (6)$$

$$\bar{f}_v(\bar{x}_k) = -\mu \nabla^2 \bar{V}(\bar{x}_k), \quad (7)$$

$$\bar{f}_p(\bar{x}_k) = \bar{\nabla} p(\bar{x}_k). \quad (8)$$

The terms above are named as acceleration force, inertial force, viscous force and pressure force. These terms are evaluated over the boundary, using the velocity and pressure fields. It must be noted that over the boundary the eulerian velocity  $\bar{v}(\bar{x})$  and the lagrangean velocity  $\bar{v}(\bar{x}_k)$  must be equal to satisfy the non-slip condition.

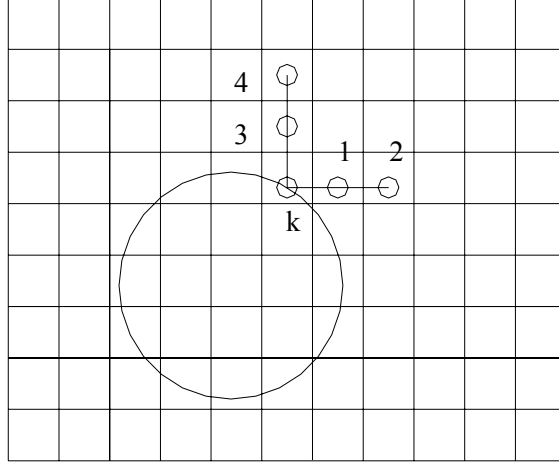


Figure 1. Interpolation scheme for velocity and pressure.

The velocity and pressure spatial derivatives are obtained from the flow quantities by the Eq. (1) and (2). Once obtained these quantities are interpolated for the grid points near the interface, as can be seen in Fig. (1).

The first and second velocity and pressure derivatives are solved using a second order Lagrange polynomial approximation, which can be written as

$$\frac{\partial \phi}{\partial x} = \frac{(x_i - x_k) + (x_i - x_2)}{(x_1 - x_2)(x_1 - x_k)} \phi_1 + \frac{(x_i - x_k) + (x_i - x_1)}{(x_2 - x_1)(x_2 - x_k)} \phi_2 + \frac{(x_i - x_1) + (x_i - x_2)}{(x_k - x_1)(x_k - x_2)} \phi_k, \quad (9)$$

$$\frac{\partial^2 \phi}{\partial x^2} = \frac{2\phi_1}{(x_1 - x_2)(x_1 - x_k)} + \frac{2\phi_2}{(x_2 - x_1)(x_2 - x_k)} + \frac{2\phi_k}{(x_k - x_1)(x_k - x_2)} \quad (10)$$

$$\frac{\partial \phi}{\partial y} = \frac{(y_i - y_k) + (y_i - y_4)}{(y_3 - y_4)(y_3 - y_k)} \phi_3 + \frac{(y_i - y_k) + (y_i - y_3)}{(y_4 - y_3)(y_4 - y_k)} \phi_4 + \frac{(y_i - y_3) + (y_i - y_4)}{(y_k - y_3)(y_k - y_4)} \phi_k, \quad (11)$$

$$\frac{\partial^2 \phi}{\partial y^2} = \frac{2\phi_3}{(y_3 - y_4)(y_3 - y_k)} + \frac{2\phi_4}{(y_4 - y_3)(y_4 - y_k)} + \frac{2\phi_k}{(y_k - y_3)(y_k - y_4)}. \quad (12)$$

Once calculated, the lagrangean force density is distributed to the nearest eulerian grid points, as can be seen in Fig. (2), by a distribution function  $D_{ij}$ . Then the Eq. (3) takes the form

$$\vec{F}_{ij} = \sum D_{ij} \vec{f}_k. \quad (13)$$

Juric (1996) suggested that  $D_{ij}$  could be given by

$$D_{ij}(\vec{x}_k) = \frac{f[(x_k - x_i)/h]f[(y_k - y_j)/h]}{h^2}, \quad (14)$$

$$f(r) = \begin{cases} f_1(r) & \text{se } \|r\| < 1 \\ \frac{1}{2} - f_1 \cdot (2 - \|r\|) & \text{se } 1 < \|r\| < 2 \\ 0 & \text{se } \|r\| > 2 \end{cases}, \quad (15)$$

with

$$f_1(r) = \frac{3 - 2 \cdot \|r\| + \sqrt{1 + 4 \cdot \|r\| - 4 \cdot \|r\|^2}}{8}, \quad (16)$$

where  $r$  is  $(x_k - x_i)/h$  or  $(y_k - y_j)/h$ , and  $h$  is the eulerian grid size.

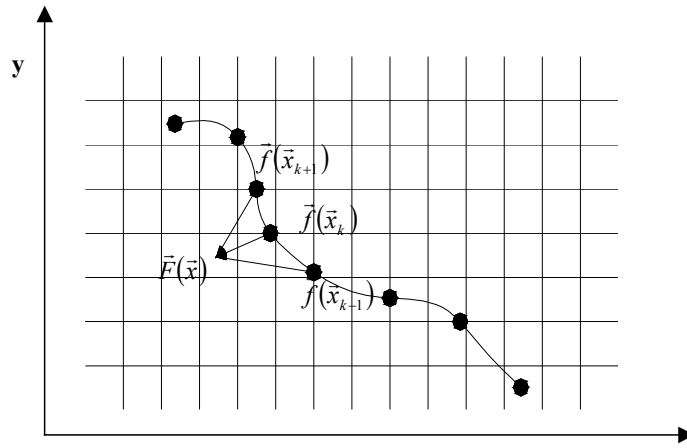


Figure 2. Force distribution process

### 3. NUMERICAL METHOD

Equations (1) and (2) were discretized using a central second order finite difference method in space and an Euler first order in time for the channel flow. For the driven cavity simulation a second order Runge-Kutta scheme was used in time.

The pressure and velocity coupling was solved by a second order pressure correction method suggested by Armfield e Street (1999) and the linear system was solved using the MSI, Modified Strongly Implicit Procedure, suggested by Schneider e Zedan (1981).

### 4. RESULTS

The Immersed Boundary Method, with the Physical Virtual Model, was applied to simulate channel and driven cavity flows in order to validate this methodology for static and moving boundaries. The channel and cavity walls were modeled using the PVM model. Figure(3) shows the physical models for the flows simulated.

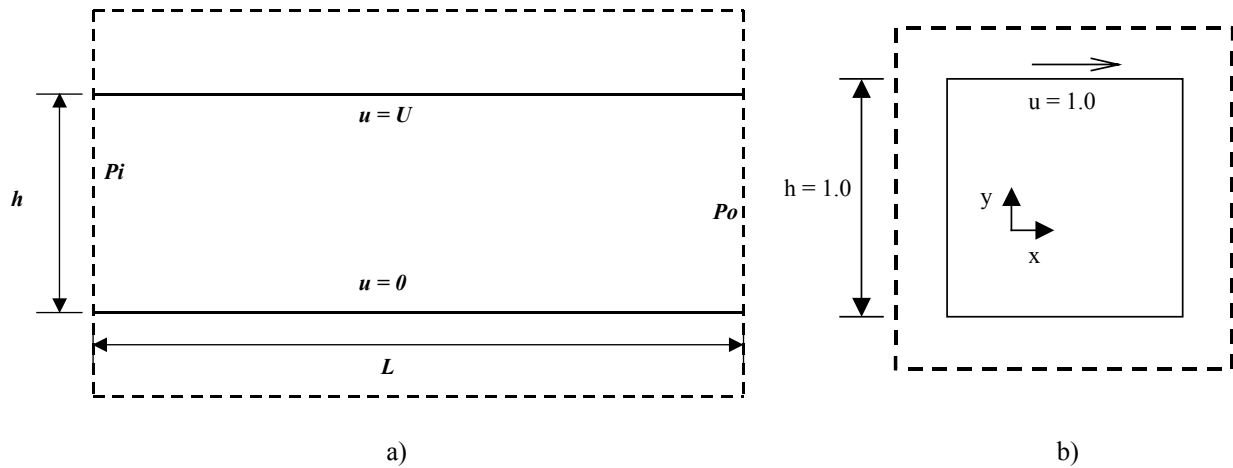


Figure 3. Physical model: a) channel; b) cavity.

#### 4.1 Couette-Poiseuille flow

The physical model for the channel can be seen in Fig. (3a). The total domain is represented by the dotted lines, where the classical boundary conditions are imposed. The domain of interested is virtually composed inside this dotted domain, and is modeled by a force field appropriately calculated. The Reynolds number is defined as a function of the height  $h$  of the channel. The channel dimensions are  $h = 0.5$ ,  $L = 2h$ .  $U$  is the upper wall velocity and  $Pi$  and  $Po$  the inflow and outflow pressure.

The Couette-Poiseuille flow was simulated and the force field for a  $Re = 250$  is presented. It is also presented the velocity profiles and the friction coefficients as a function of Reynolds number. Comparisons with analytical solutions were performed. The flow conditions for this flow are listed in Tab. (1).

Figure (4) shows the force field. It can be seen that as the upper wall velocity has a different value from the lower wall velocity, the force is also different, with a higher force (in modulus) at the lower wall, and a lower force at the upper wall.

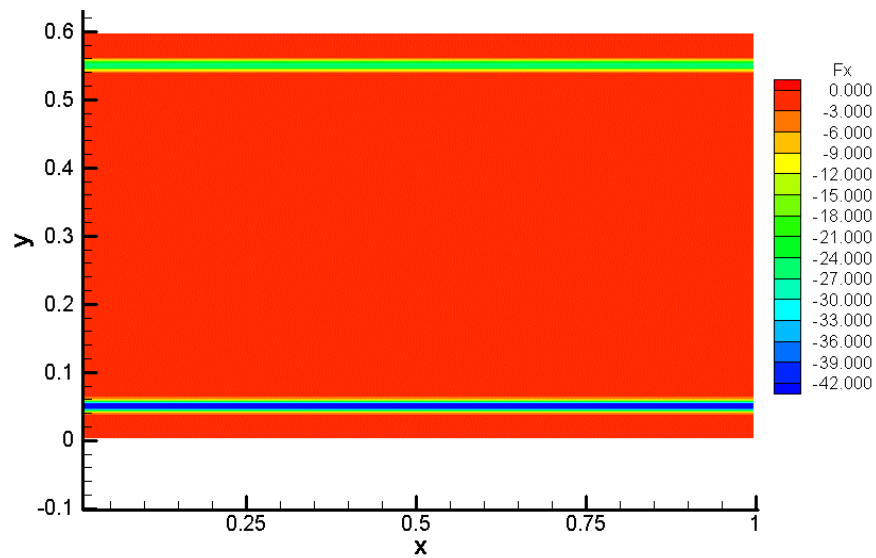


Figure 4. Force field - Re 250

Table 1. Couette-Poiseuille flow conditions

Re	$U$	$\Delta P = P_o - P_i$	$\nu$
100	1,0	- 0,72	0,01
250	1,0	- 2,16	0,01
500	1,0	- 4,56	0,01
750	1,0	- 6,96	0,01

The velocity results are shown in Fig. (5a), and (5b). The maximum velocity occurs above the central line of the channel, as could be predicted by the analytical solution. The maximum error is of 1%. It can be noted the pressure gradient influence over the flow. As higher is the pressure gradient, more closely to a parabolic shape and less asymmetric is the velocity profile. There is a good agreement between the numerical and analytical results.

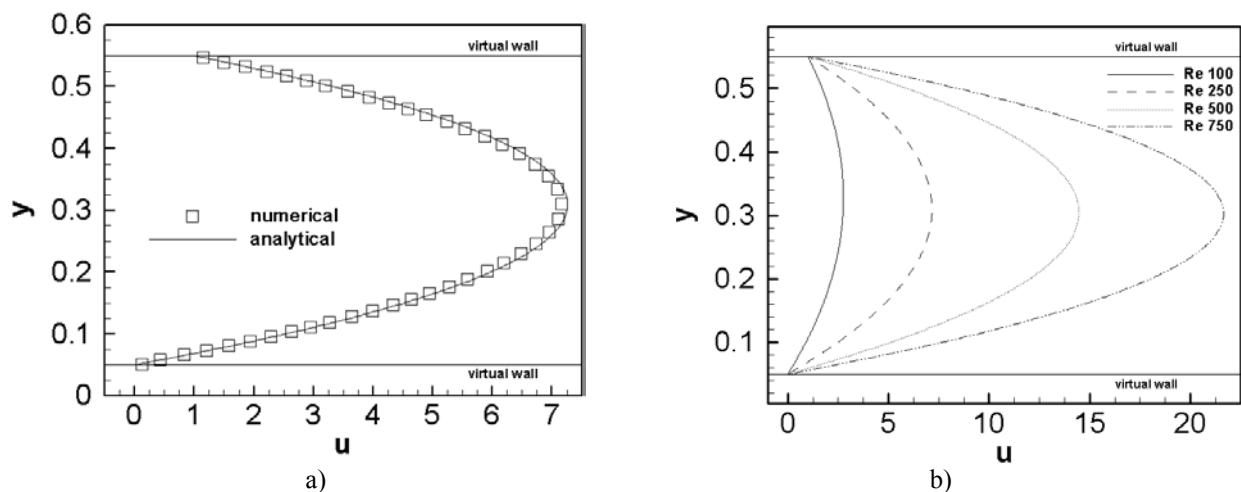


Figure 5. Velocity profiles: a) numerical x analytical velocity – Re = 250; b) as a function of Re number.

The friction coefficient was obtained numerically, and a comparison with the analytical calculation was performed. The analytical friction coefficient,  $f_s$ , is defined as

$$f = \frac{\tau_{yx}}{\frac{1}{2}\rho\bar{u}^2}, \quad (17)$$

where  $\tau_{yx}$  is the shear stress and  $\bar{u}$  is the mean velocity. The analytical shear stress is given as

$$\tau_{yx} = \mu \frac{\partial u}{\partial y}. \quad (18)$$

The numerical shear stress is calculated multiplying the eulerian force per volume over the boundary with the grid size  $dx$ . It must be noted that in force calculation, the results are for the two sides of the virtual wall. More clearly, there are flows at both sides of the channel wall. Thus for the analytical shear stress calculation it must be considered the flow in all domain. The friction coefficient is defined as a function of the total shear stress at the wall and the mean velocity in the main channel.

Figure (6a) shows that, in Couette-Poiseuille flow, two friction coefficients are obtained. This occurs because there are two different shear stress values, one for the upper wall, due to its movement and the pressure gradient, and the other for the lower wall, due only to the pressure gradient.

It can be noted again in Fig. (6b) the Re number influence over the friction coefficients. As the Re increases, both the friction coefficient decreases up to a value close to null.

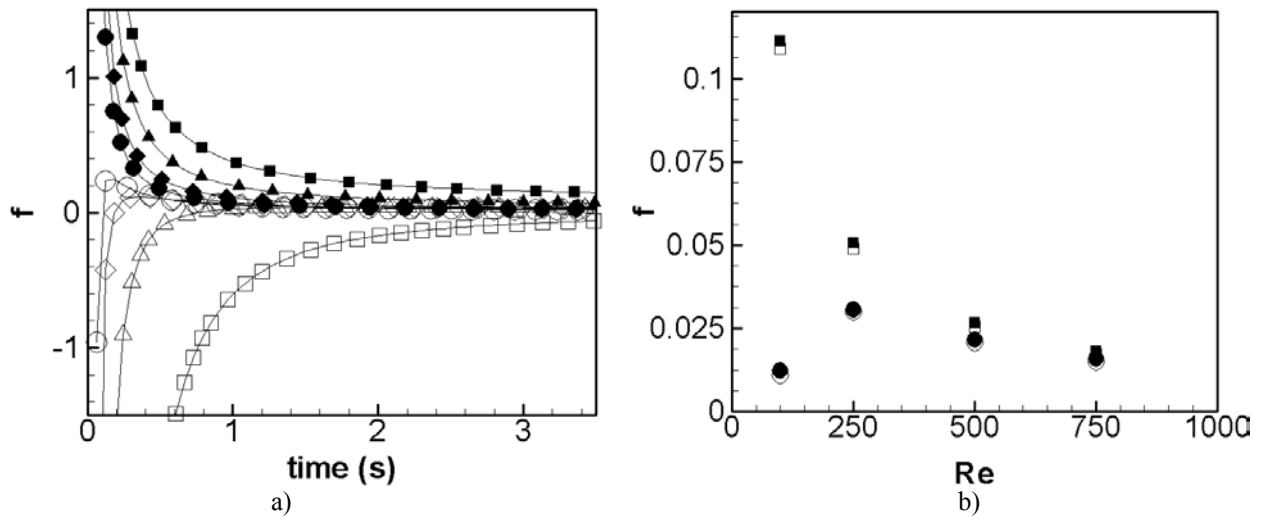


Figure 6. a) Friction coefficients: square - Re 100, delta - Re 250, diamond - Re 500, circle -Re 750.; filled symbols - lower wall, not filled - upper wall; b) friction coefficients x Re; square - lower wall; circle - upper wall; filled symbols - numerical, not filled - analytical

#### 4.2 Driven Cavity

The driven cavity is an interesting problem for testing and evaluating numerical techniques once it has singularities at its lower corners. The physical model for the present simulation consists in a square cavity of unity height and length, and it can be seen in Fig. (3). The vertical and lower walls have a null velocity in both  $x$  and  $y$  directions. The upper wall has a unity velocity in  $x$  direction and a null velocity in  $y$  direction. This problem was simulated for two different Reynolds number, 400 and 1000. The whole domain is discretized by a  $100 \times 100$  regular mesh. The cavity interior is composed by a  $50 \times 50$  regular mesh. Again the Reynolds number is based in the cavity height. The results achieved were compared with Ghia et al. (1982) and Hou et al. (1995) ones.

Important results for the driven cavity problem are the velocity profiles through the cavity geometric center. These profiles are present in Fig. (7), where one can see the present result confronted with Ghia et al. (1982) ones. It can be seen a good agreement within the results in both cases of Re 400 and 1000. An important fact is that for a higher Re value the boundary layer at the wall is thinner than that in the case of lower Re. Another aspect in these profiles is its close linearity in the central core, what indicates the developing of an uniform vorticity field.

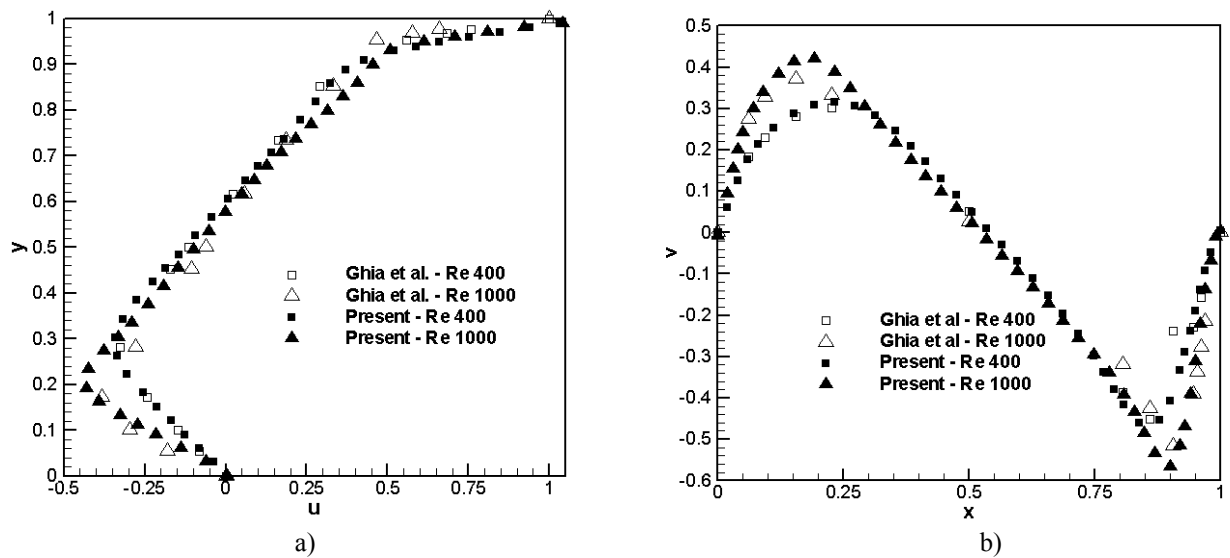


Figure 7. Velocity profiles: a) u-velocity along vertical center line; b) v-velocity along horizontal center line.

The streamlines patterns for both cases are shown in Fig. (8). Although the present results are in good agreement with the reference ones, for Re 400 the present simulation did not capture the secondary left vortex. One possible cause for this is the coarse grid used inside the cavity (50x50), while Ghia et al (1982) used a 129x129 mesh and Hou et al. (1995) used a 256x256 lattice. However it can be seen at this lower corner a different behavior by the streamlines.

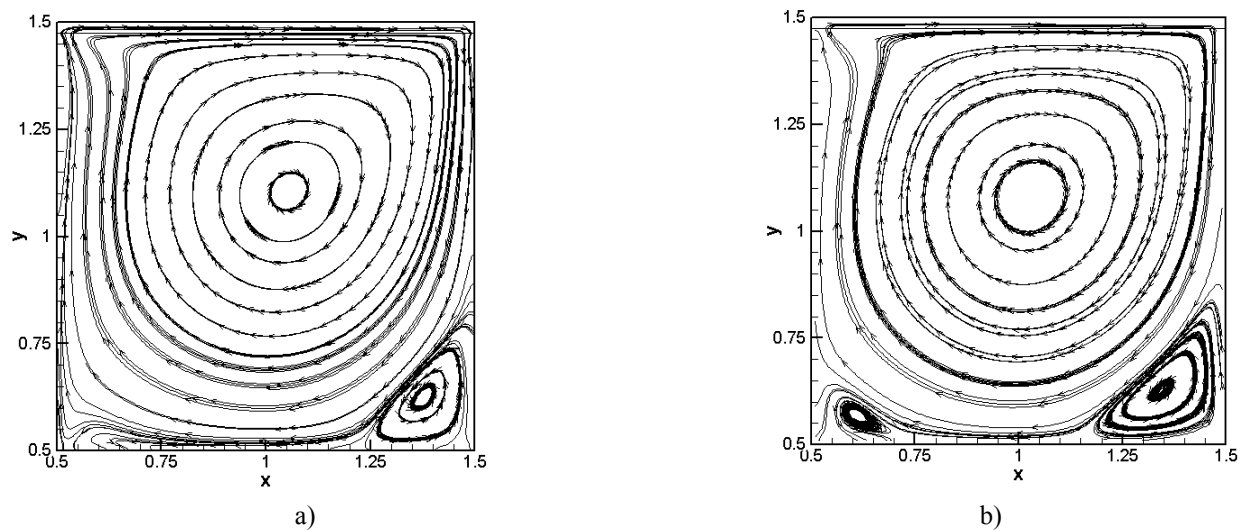


Figure 8. Streamlines pattern: a) Re 400; b) Re1000.

The primary vortice center for Re 1000 is closer to the cavity geometric center, while for Re 400 primary vortice center is close to the right top corner. Excluding the secondary left vortice for Re 400, all the vortices center of the present simulation are in good agreement with the reference results, as shown in Tab. (2).

Table 2. Vortice center location

Re		Primary vortice		Secondary vortice - left		Secondary vortice - right	
		x	y	x	y	x	y
400	Ghia et al.	0.5547	0.6055	0.0508	0.0469	0.8906	0.1250
	Hou et al.	0.5608	0.6078	0.0549	0.0510	0.8902	0.1255
	Present	0.55	0.60			0.88	0.12
1000	Ghia et al.	0.5313	0.5625	0.0859	0.0781	0.8594	0.1094
	Hou et al.	0.5333	0.5647	0.0902	0.0784	0.8667	0.1137
	Present	0.53	0.58	0.61	0.57	0.84	0.13

The pressure contours are displayed in Fig. (9). A comparison with the Hou et al (1995) results shows a good agreement. It must be noted that the Navier-Stokes equations involve a pressure gradient, so that identical pressure values are unexpected. Thus this result is more qualitative rather than quantitative.

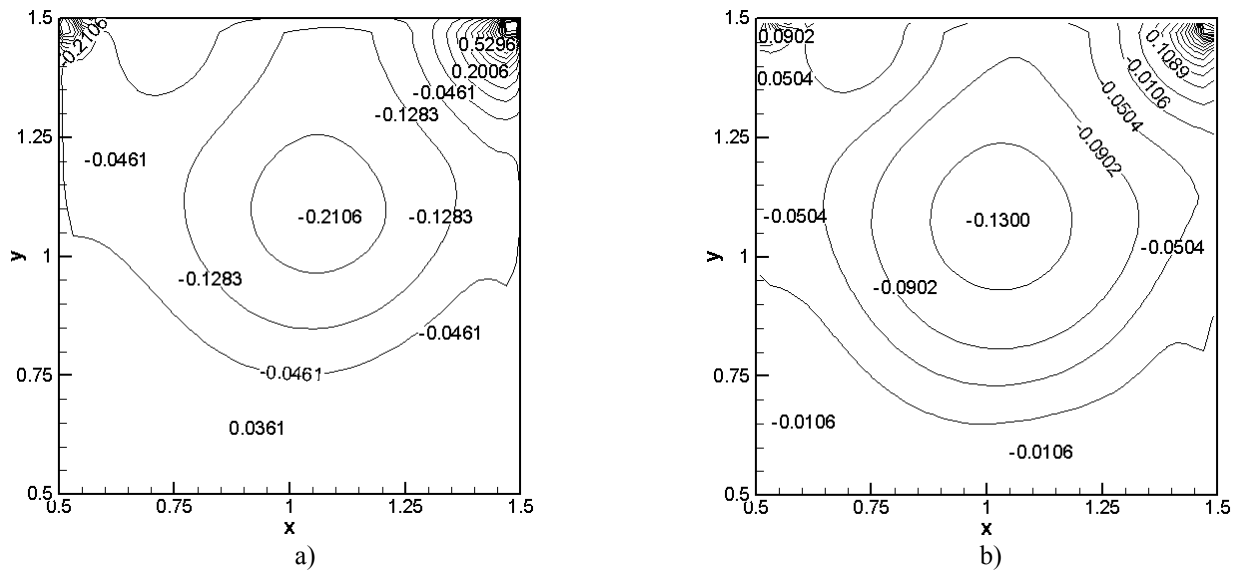


Figure 9. Pressure contours: a) Re 400; b) Re 1000.

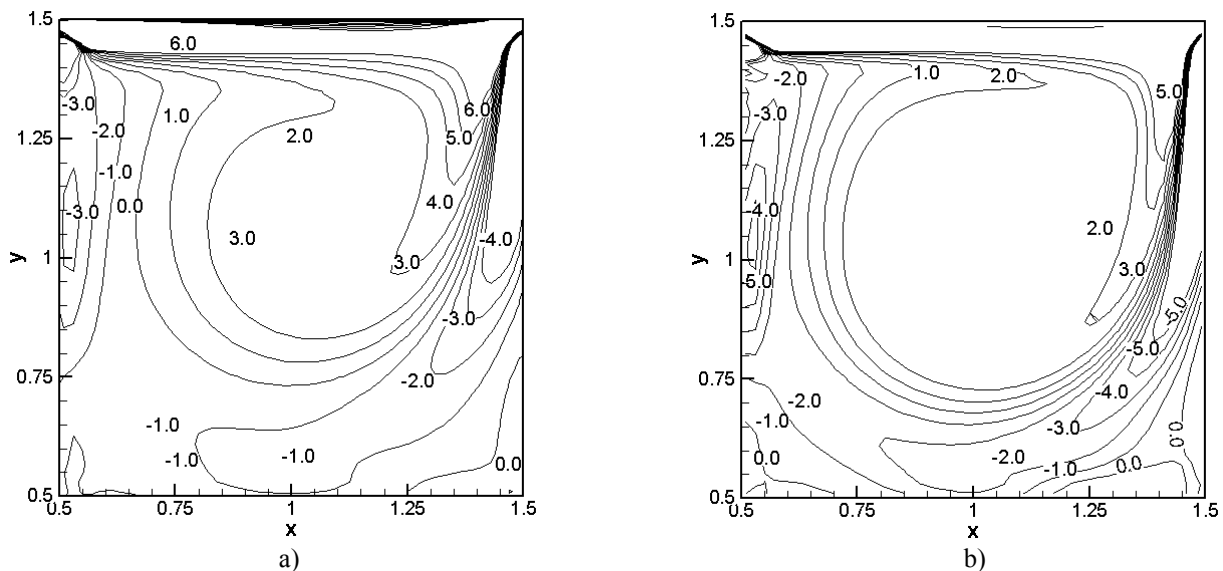


Figure 10. Vorticity contours: a) Re 400; b) Re 1000.

Figure (10) shows the vorticity contours obtained for the driven cavity problem. One can see that for the higher Re value there are more regions of high vorticity gradients, a central core with vorticity close to a constant value and the viscous effects are restricted to thin shear layers close to the walls. For the case of Re 400 the region of uniform vorticity is smaller and the vorticity gradients are smoother. These results strongly agree with the two references results.

## 5. CONCLUSIONS

The methodology proposed permits to obtain results that have good agreement with the analytical solutions, for the channels flows cases, and with the numerical solution, for the driven cavity case. The errors for the channel simulation were in a order of 1%. These results permit to advance in order to implement the methodology for more complex geometries, such as channel over cavities and flow chambers with moving boundaries.

## 6. ACKNOWLEDGEMENTS

This work was supported by CNPq (Brazilian Research Council).

## 7. REFERENCES

- Arruda, J. M., Lima e Silva, A. L. F., Silveira-Neto, A. and Roma, A. M., 2002, “Aplicação de Dinâmica dos Fluidos Computacional em Problemas de Bioengenharia”. Proceedings of the 3rd Transition and Turbulence Spring School, a-22, Florianópolis, Brazil. – In Portuguese.
- Armfield, S. and Street, R., 1999, “The Fractional-Step Method for the Navier-Stokes on Staggered Grids: the Accuracy of Three Variations”. *NOTE. Journal of Computational Physics*, No. 153, 660-665.
- Fadlun, E. A., Verzicco, R., Orlandi, P., and Mohd-Yusof, J., 2000, “Combined Immersed-Boundary Finite-Difference Methods for Three-dimensional Complex Flow Simulations”, *Journal of Computational Physics*, No. 161, pp. 35-60.
- Ghia, U., Ghia, K. N. and Shin, C. T., 1982 “High-Re Solutions for Incompressible Flow Using the Navier-Stokes Equations and a Multigrid Method”, *Journal of Computational Physics*, No. 48, pp. 387-411.
- Goldstein, D., Hadler, R. and Sirovich, L., 1993 “Modeling a no-Slip Flow Boundary with an External Force Field”, *Journal of Computational Physics*, No. 105, pp. 354-.
- Harlow, F. H. and Welch, J. E., 1965, “Numerical Calculation of Time-Dependent Viscous of Incompressible Flow of Fluid with Free Surface”, *Physics Fluids*, 8, pp. 2182-2189.
- Hou, S., Zou, Q., Chen, S., Doolen, G. and Cogley, A. C. E., 1995, “Simulation of Cavity Flow by the Lattice Boltzmann Method”, *Journal of Computational Physics*, No. 118, pp. 329-347.
- Juric, D., 1996, “Computation of Phase Change”, Ph.D. Thesis, Mechanical Engineering, University of Michigan.
- Lima e Silva, A. L. F., Silveira-Neto, A. and Damasceno, J. J. R., 2003, “Numerical Simulation of Two Dimensional Flows over a Circular Cylinder Using the Immersed Boundary Method”, *Journal of Computational Physics*, No 189, pp. 351-370.
- Peskin, C.S., 1977, “Numerical analysis of Blood Flow in the Heart”, *Journal of Computational Physics*, No. 25, pp. 220-252
- Schneider, G E., and Zedan, M., 1981, “A modified strongly implicit procedure for the numerical solution of field problems”. *Numerical Heat transfer*, No. 4, 1-19.

## 8. Copyright Notice

The author is the only responsible for the printed material included in his paper.